Proceedings of the International School and Conference on Optics and Optical Materials, ISCOM07, Belgrade, Serbia, September 3–7, 2007

Optodynamic Characterization of Laser-Induced Bubbles

P. Gregorčič* and J. Možina

Faculty of Mechanical Engineering, University of Ljubljana
Aškerčeva 6, 1000 Ljubljana, Slovenia

Laser-induced bubbles can be caused by an optical breakdown in water. They are a result of the optodynamical process where the energy of a high intensity laser pulse is converted into the mechanical energy through an optodynamic conversion. At this process the absorbed optical energy causes plasma expansion that in turn initiates dynamic phenomena: spreading of a shock wave and the development of a cavitation bubble. When the cavitation bubble reaches its maximum radius it starts to collapse due to the pressure of the surrounding liquid. This collapse in turn initiates a new bubble growth and bubble collapse. The process therefore repeats itself, resulting in so-called cavitation-bubble oscillations, with a new shock wave being emitted after every collapse. We present an optodynamic characterization of cavitation bubble's oscillations based on a laser beam-deflection probe. Employed setup enabled us one- or two-dimensional scanning with deflections of a laser probe beam. Deflections were detected with a fast quadrant photodiode.

PACS numbers: 42.62.–b, 47.40.–x, 47.55.dd

1. Introduction

Cavitation bubbles can be produced by a high intensity laser pulse focused in water [1]. When the pulse intensity reaches the breakdown threshold, plasma — a "gas" of charged particles — occurs in the breakdown region [2]. Since such a plasma is a strong absorber of the laser light [3], the energy of the laser pulse is converted into the mechanical energy through an optodynamic conversion. At this optodynamical process the absorbed optical energy causes plasma expansion followed by dynamic phenomena: emitting of a shock wave and the development of a cavitation bubble. When the cavitation bubble reaches its final radius it starts to collapse due to the pressure of the surrounding water. This collapse in turn initiates a new bubble growth and bubble collapse. The process therefore repeats

*corresponding author; e-mail: peter.gregorcic@fs.uni-lj.si

itself, resulting in so-called cavitation-bubble oscillations, with a new shock wave being emitted after every collapse.

Cavitation bubbles as well as shock waves are interesting due to ocular microsurgery, where Q-switched lasers with ns pulse durations are commonly used to vaporize the tissue in procedure such as a cataract removal [4]. Understanding the development of the cavitation bubble and the pressure front, their dynamics and propagation is important to avoid adverse effects on the eye during ophthalmology procedure based on laser surgery [5].

We present an optodynamic characterization of cavitation bubble's oscillations based on laser beam-deflection probe (BDP) [6]. This method is grounded on measurements of deflections of the laser beam. When the shock wave or cavitation bubble cross the path of the probe, the refractive-index gradient results in a measurable deflection of the probe beam [7, 8]. These beam deflections can be detected with a position-sensing photodetector such as a quadrant photodiode. Such a method can be used in various applications, such as cavitation-bubble measurements [9], plasma characterization [10], or monitoring of the laser drilling of through-holes in glass [11].

Employed setup enabled us one- or two-dimensional scanning with deflections of a laser probe beam. Deflections were detected with a fast quadrant photodiode. From BDP signals times of flights for cavitation bubble during its expansion as well as its collapse were determined. From maximum bubble's radius the energy converted form the laser pulse energy into the mechanical energy of the cavitation bubble were estimated for the first three oscillations. Measured bubble dynamics was compared with Rayleigh–Plesset theory [12, 13].

2. Theory

The study of bubble dynamics in a liquid is greatly simplified by the assumption of spherical symmetry. Such a bubble collapse in an infinitely large and incompressible liquid can be roughly described by the Rayleigh model [12], which considers that the liquid's pressure as well as the pressure inside the bubble are constant during its collapse. With this assumption Rayleigh deduced the variation of the bubble's radius with time from the kinetic energy of the motion and the work done by the pressure

$$U^2 = \frac{2p_0}{3\rho}\left(\frac{R_{\max}^3}{R^3} - 1\right). \tag{1}$$

Here, $U = \mathrm{d}R/\mathrm{d}t$ is the velocity of the bubble's boundary, $R_{\max}$ is the maximum radius, p_0 is the liquid's pressure and ρ is the liquid's density. The bubble's collapse time can be obtained by integrating Eq. (1). With substitution $\xi = R/R_{\max}$ we get

$$T_{\mathrm{C}} = R_{\max}\sqrt{\frac{3\rho}{2p_0}}\int_0^1 \frac{\xi^{3/2}}{\sqrt{1-\xi^3}}\mathrm{d}\xi = 0.915 R_{\max}\sqrt{\frac{\rho}{p_0}}. \tag{2}$$

The collapse time of a spherical cavitation bubble in an infinite liquid is

therefore proportional to its maximum radius. Even though the Rayleigh model is a relatively simple model for cavitation-bubble oscillations, Eq. (2), which describes the relationship between the collapse time and the maximum radius, it was verified and is still used by many authors [9, 14]. Assuming that the expansion and collapse of the bubble are symmetrical processes, the oscillation time T_{O}, i.e., the time between the bubble's appearance and its collapse, can be expressed as $T_{\mathrm{O}} = 2T_{\mathrm{C}}$. This assumption is valid when the duration of the laser pulse is much shorter than the bubble's oscillation and the viscosity of the liquid is negligible [3].

A cavitation bubble's energy, E_{B}, is proportional to the cube of its maximum radius [15]:

$$E_{\mathrm{B}} = \frac{4\pi p_0}{3} R_{\mathrm{max}}^3. \tag{3}$$

A bubble's energy is also approximately proportional to the energy of the breakdown pulse, E_{L} [15], so $E_{\mathrm{B}} = \eta E_{\mathrm{L}}$. Here, η is the share of the pulse's energy converted into the bubble's energy.

3. Experimental setup

Experimental setup is shown in Fig. 1. The breakdown was induced in distilled water using a Q-switched Nd:YAG laser ($\lambda = 1064$ nm), designed for ocular photodisruption. The duration of the laser pulse was 7 ns, while the pulse energies used in our experiments were between 1.63 and 8.6 mJ. The estimated beam's waist radius in the water was ≈ 30 μm, so the intensities of the pulses were in the range of $1{-}4 \times 10^{14}$ W m^{-2}. The threshold energy, E_{th}, for distilled water used in our experiments was measured as is described in [6] and was $E_{\mathrm{th}} = 1.1 \times (1 \pm 0.3)$ mJ. Therefore the dimensionless parameter $\beta = E_{\mathrm{L}}/E_{\mathrm{th}}$, showing the ratio between the laser energy and the threshold energy, was between $\beta \approx 1.5$ and $\beta \approx 7.8$.

BDP scanning bases on measurements of time of flight, i.e., the time that takes from the shock wave or cavitation bubble to reach the probe beam at particular position. He–Ne laser ($\lambda = 633$ nm) was used as a probe beam. Its beam was led through the optics to achieve small beam waist radius (≈ 3 μm). When the shock wave or cavitation bubble cross the path of such a probe, the refractive-index gradient results in a measurable deflection of the beam [7, 8]. These deflections were measured with a fast quadrant photodiode, having the rise time ≈ 4 ns. Typical signals from the probe showing the shock waves and cavitation bubble during its expansions and collapses are described elsewhere [6, 9]. The small beam diameter and the high-frequency bandwidth of the probe were necessary in order to achieve a high temporal as well as spatial resolution.

The BDP measurements of cavitation bubble were made in the horizontal direction (left–right) (see also Fig. 1), i.e., perpendicular to the optical axes of the breakdown beam. The shift during scanning was 30 μm, while the shift used for measurements of the bubble's maximum radius was in the range of 10–30 μm. The

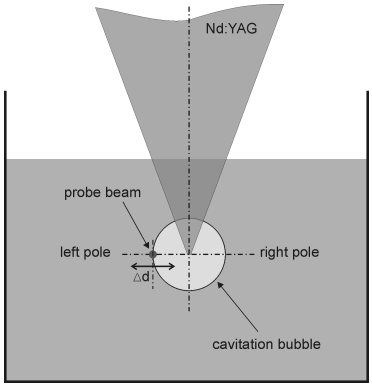

Fig. 1. Experimental setup. The breakdown was induced by a Nd:YAG laser pulse that was focused into the vessel containing the distilled water. BDP scanning in horizontal direction (left–right), i.e., perpendicular to the Nd:YAG optical axis, was used as a measurement method. A He–Ne laser was used as a probe beam.

applied positioning system for moving the laser probe relative to the breakdown region enabled a shift down to 1 μm. The experimental setup was automatically controlled with the specially developed software that also enabled data acquisition from a digital oscilloscope (500 MHz Wave Runner 6050A, LeCroy), as well as data processing.

4. Results and discussion

A movement of the left (circles) and the right (squares) bubble's pole is shown in Fig. 2. The breakdown laser energy was $4.7 \times (1 \pm 0.3)$ mJ ($\beta \approx 4.3$). The presented data were processed using a method for reducing the measurement noise of the BDP scanning technique [9]. Vertical axis presents the bubble's radius and corresponds to the position of the probe beam relative to the breakdown site (i.e., cavitation bubble source) during the scanning procedure. The time for each particular radius was obtained from the beam deflection signal corresponding to the current position of the probe beam. Each oscillation attained smaller maximum radius, since the bubble's energy is lost due to the emission of a shock wave after every collapse, the heat conduction and the liquid's viscosity.

Velocity of the bubble's wall can be determined from the first derivative of the measurements showing bubble's radius evolution. Figure 3 shows bubble's wall velocity during bubble's expansion as well as during its collapse. The dimensionless radius $R/R_{\max}$ is presented in horizontal axes. It is important to note that the logarithmic scale is used in vertical axes for better presentation. It is shown that velocities at small bubble radii, i.e., immediately after the breakdown and close to the collapse reaches values up to ≈ 800 m/s. On the other hand, the velocities for $R > 0.67R_{\max}$ are below 10 m/s. Solid line in Fig. 3 shows Rayleigh's model (see Eq. (1)) for $p_0 = 1$ bar and $\rho = 10^3$ kg m^{-3}. It is evident that the model

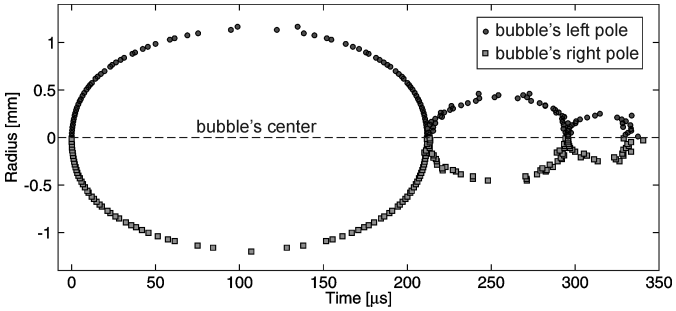

Fig. 2. A movement of the left (circles) and the right (squares) bubble's pole, measured by BDP scanning. The energy of the breakdown laser was 4.7 mJ.

equals experimental data since the radius of the bubble is larger than $0.4R_{\max}$. On the other hand, at radii larger than $0.15R_{\max}$ the model starts to deviate from measured velocities. In this case all assumptions are broken, since this relatively simple model predicts that velocity increases to infinity when the radius goes against zero.

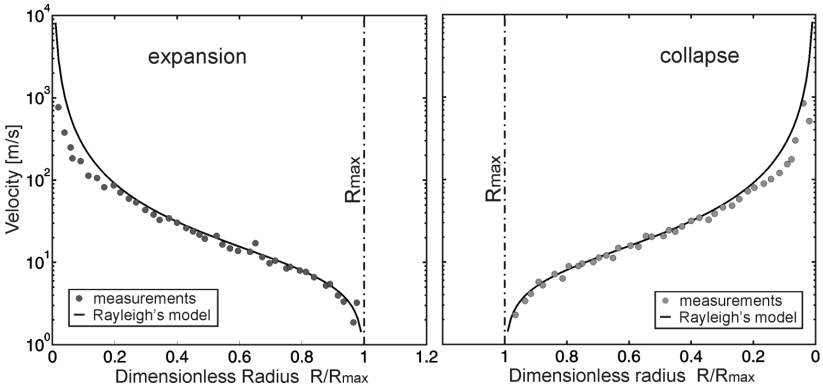

Fig. 3. Velocity of the bubble's wall as a function of dimensionless radius is shown for the bubble's expansion and collapse. A logarithmic scale is used on the vertical axis. Rayleigh's model for $p_0 = 1$ bar and $\rho = 10^3$ kg m^{-3} is shown with a solid line.

Figure 4 shows the maximum radius of the first bubble's oscillation vs. laser pulse energy. Solid line shows the fit of Eq. (3). It can be concluded that measurements are in a good agreement with theory. Therefore on this basis we were able to calculate the share of the laser-pulse energy converted into the mechanical energy of the cavitation bubble $E_{\mathrm{b}1}$. The results are presented in Table; they show that the share η of the optical energy converted into the bubble's energy was in the range 13–19%. Additionally, Table shows the energies of the second $E_{\mathrm{b}2}$ and the third $E_{\mathrm{b}3}$ oscillations as well as the shares of the first oscillation's energy converted into the energy of the second $E_{\mathrm{b}2}/E_{\mathrm{b}1}$ and the third oscillation $E_{\mathrm{b}3}/E_{\mathrm{b}1}$. Vogel et

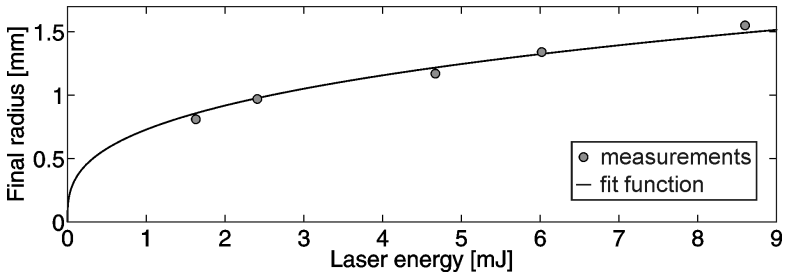

Fig. 4. Maximum bubble's radius versus breakdown laser energy. Solid line presents fit function (see Eq. (3)) for $p_0 = 1$ bar.

TABLE

Calculated energies for the first (E_{b1}), second (E_{b2}) and third (E_{b3}) oscillation. The shares of the laser-pulse energy converted into the bubble's energy η as well as the shares of the first bubble's energy converted into the energy of the second and the third oscillations are also shown.

E_{L} [mJ]	E_{b1} [μJ]	η	E_{b2} [μJ]	$E_{\mathrm{b2}}/\mathrm{E_{b1}}$	E_{b3} [μJ]	$E_{\mathrm{b3}}/E_{\mathrm{b1}}$
8.60±0.23	1600±180	19%±3%	131±23	8.2%±3%	25±6	1.56%±0.6%
6.0±0.12	1000±130	17%±3%	86±17	8.6%±3%	14±4	1.4%±0.6%
4.7±0.16	670±100	14%±3%	46±12	6.9%±3%	6.5±2	0.97%±0.4%
2.41±0.07	380±60	16%±3%	16±4	4.2%±2%	2.9±1.8	0.76%±0.6%
1.63±0.04	220±40	13%±3%	9.2±3	4.2%±2%	1.4±1.1	0.64%±0.6%

al. [16] found that the energy loss due to the emission of a shock wave represents between 70% and 90% of the energy losses. Therefore, from the results presented in Table, the energies carried off with the second and the third shock waves can be estimated as 64–86% and 4–6% of the first bubble's oscillation energy, respectively. From the application point of view, shock-wave energy is important since its range — in contrast to that of the cavitation bubble — is not limited to the vicinity of the breakdown region.

5. Conclusion

We have presented measurements of laser-induced cavitation bubbles using a laser-beam deflection probe. From the bubble's radius evolution we also calculated bubble's wall velocities during expansion and collapse. Measured data were compared with the Rayleigh model. A good agreement with the model was shown for the case that the bubble's radius is larger than $0.15R_{\mathrm{max}}$. From final bubble radii we also calculated energies of bubble's oscillations. Shares of the optical energy converted into the mechanical energy of the cavitation bubble as well as the shares of the first bubble's energy carried off with the second and the third shock waves were also estimated.

References

[1] W. Lauterborn, H. Bolle, *J. Fluid Mech.* **72**, 391 (1975).

[2] P.K. Kennedy, *IEEE J. Quantum Elect.* **31**, 2241 (1995).

[3] A. Vogel, S. Busch, U. Parlitz, *J. Acoust. Soc. Am.* **100**, 148 (1996).

[4] A. Vogel, *Phys. Med. Biol.* **42**, 895 (1997).

[5] R. Petkovšek, G. Močnik, J. Možina, *Fluid Phase Equilib.* **256**, 158 (2007).

[6] R. Petkovšek, P. Gregorčič, J. Možina, *Meas. Sci. Technol.* **18**, 2972 (2007).

[7] G.P. Davidson, D.C. Emmony, *J. Phys. E, Sci. Instrum.* **13**, 92 (1980).

[8] J. Diaci, *Rev. Sci. Instrum.* **63**, 5306 (1992).

[9] R. Petkovšek, P. Gregorčič, *J. Appl. Phys.* **102**, 044909 (2007).

[10] M. Villagrán-Muniz, H. Sobral, R. Navarro-González, *Meas. Sci. Technol.* **14**, 614 (2003).

[11] R. Petkovšek, A. Babnik, J. Diaci, *Meas. Sci. Technol.* **17**, 2828 (2006).

[12] L. Rayleigh, *Philos. Mag.* **34**, 94 (1917).

[13] M.S. Plesset, *J. Appl. Mech.* **16**, 277 (1949).

[14] D. Obreschkow, P. Kobel, N. Dorsaz, A. de Bosset, C. Nicollier, M. Farhat, *Phys. Rev. Lett.* **97**, 094502 (2006).

[15] A. Vogel, J. Noack, K. Nahen, D. Theisen, S. Busch, U. Parlitz, D.X. Hammer, G.D. Noojin, B.A. Rockwell, R. Birngruber, *Appl. Phys. B* **68**, 271 (1999).

[16] A. Vogel, W. Lauterborn, R. Timm, *J. Fluid Mech.* **206**, 299 (1989).